Journal of Alloys and Compounds 509 (2011) 5290–5294

Contents lists available at ScienceDirect

Journal of Alloys and Compounds

journal homepage: www.elsevier.com/locate/jallcom

The role of pH and boron doping on the characteristics of sol gel derived ZnO films

Saliha Ilican[a,*], Fahrettin Yakuphanoglu[b], Mujdat Caglar[a], Yasemin Caglar[a]

[a] Anadolu University, Faculty of Science, Department of Physics, 26470 Eskisehir, Turkey
[b] Firat University, Faculty of Arts and Sciences, Department of Physics, 23169 Elazig, Turkey

ARTICLE INFO

Article history:
Received 23 November 2010
Received in revised form 10 January 2011
Accepted 19 January 2011
Available online 15 February 2011

Keywords:
B doped ZnO
Sol gel spin coating
pH effect
FESEM
Absorption edge shift

ABSTRACT

Undoped and boron doped ZnO films (nominal volume B/Zn ratio = 1%, 3% and 5%) were deposited onto glass substrates by the sol gel method using spin coating technique. Zinc acetate dihydrate (ZnAc), 2-methoxyethanol and monoethanolamine (MEA) were used as a starting material, solvent and stabilizer, respectively. Trimethyl borate (TMB) was used as a dopant source. The pH value of the sol was adjusted with glacial acetic acid and ammonia and it changed from acid to base in nature. The effect of pH value and B dopant on the structural, morphological and optical properties of the films was investigated. The crystalline structure and orientation of the films were investigated using XRD study. The crystallite size of the films was determined. The XRD analyses showed that the undoped ZnO film crystallinity enhanced when pH of the precursor sol was increased from 5.05 to 7.00. Surface morphology was studied by a field emission scanning electron microscope (FESEM), and the effects of the doping concentration and pH values on the microstructure of the films were investigated. The optical band gap values on the surface morphology of the films were determined. The absorption edge shifted depending on the pH values and the B dopant.

1. Introduction

Semiconducting nanomaterials have attracted considerable attention due to their novel functionalities [1,2]. Zinc oxide (ZnO) is emerging as a material of interest for a variety of electronic applications such as varistors, gas sensors, transparent electrodes, and thin film transistor [3–7]. It can be used in a large number of areas, and unlike many of the materials with which it competes, ZnO is inexpensive, relatively abundant, chemically stable, easy to prepare and non-toxic. As an interesting chemically and thermally stable n-type semiconductor, ZnO has a large exciton binding energy of 60 meV and wide band gap energy of 3.37 eV at room temperature. The non-stoichiometric ZnO thin films usually exhibit n-type behavior with low resistivity due to the oxygen vacancies and zinc interstitials.

In spite of extensive studies on preparation, properties and effects of dopants on the properties of ZnO, certain effects of either some dopants or preparation procedures are still remaining unclear. Unlike the effects of In [8,9], Al [10,11], Sn [12,13], F [14,15] elements in ZnO, the effect of boron (B) is less discussed.

B doped ZnO films can be deposited by several methods such as metal organic chemical vapor deposition [16,17], DC sputtering [18], pulsed laser deposition (PLD) [19], chemical vapor deposition technique [20], spray pyrolysis [21,22], vacuum arc plasma evaporation [23], and sol gel [24,25]. Among these methods, the sol gel method is one of the most commonly used method for preparation of transparent and conducting oxides owing to its simplicity, safety, non-vacuum system of deposition and hence inexpensive method for large area coatings. Other advantages of the sol gel method are that it can be adapted easily for production of large-area films, and to get varying band gap materials during the deposition process.

Despite these advantages, according to our knowledge there are few reports about boron doped ZnO which is particularly prepared by sol gel. Especially for boron doped ZnO films, to investigate the effect of doping, it is important to discover the amount of reagents to be added to the sol to obtain the best quality films. So, in this paper, we report the effect of both B doping and pH on the structural, morphological and optical properties of the ZnO films.

2. Experimental

Undoped and B doped ZnO films were prepared by the sol gel method by using spin coating technique. Zinc acetate dihydrate (ZnAc), 2-methoxyethanol and monoethanolamine (MEA) were used as a starting material, solvent and stabilizer, respectively. Trimethyl borate (TMB) was used as a dopant source. These solutions of 0.5 M were mixed together in nominal volume ratio of the B/Zn (0%, 1%, 3% and 5%). The molar ratios of ZnAc and TMB to MEA were maintained at 1:1. The pH of the as-prepared ZnAc sol was measured as 6.80. Glacial acetic acid or ammonia was added to ZnAc sol drop by drop under constant stirring until the pH values reached 5.05, 5.77, 7.00 and 7.15. The pH values of the premixed sols in nominal different

* Corresponding author. Tel.: +90 222 3350580; fax: +90 222 3204910.
E-mail addresses: silican@anadolu.edu.tr, silican@semiconductorslab.com (S. Ilican).

0925-8388/$ – see front matter © 2011 Elsevier B.V. All rights reserved.
doi:10.1016/j.jallcom.2011.01.122

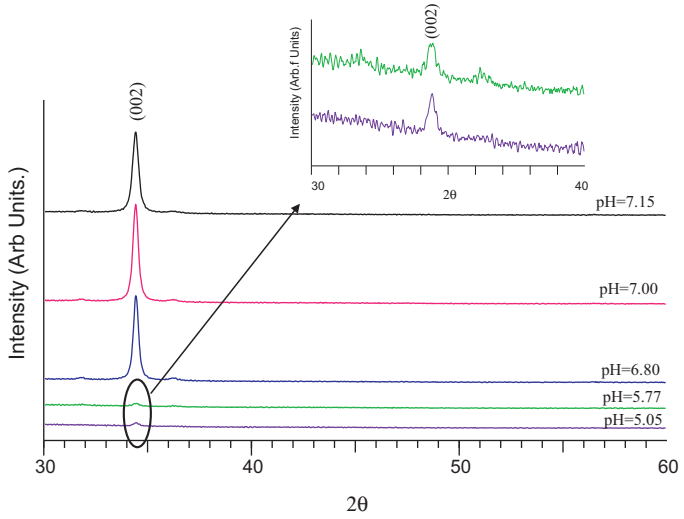

Fig. 1. XRD spectra of the undoped ZnO films for the different pH values.

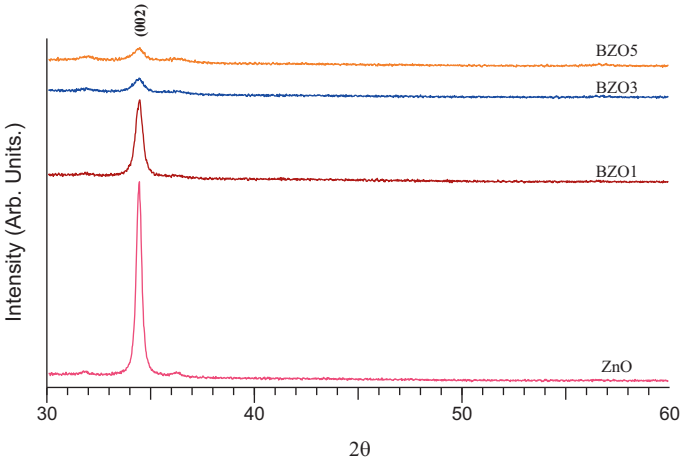

Fig. 2. XRD spectra of the undoped and B doped ZnO films at pH = 7.00.

volume ratios (B/Zn = 1%, 3% and 5%) were adjusted to 7.00. The obtained sols were stirred at 50 °C for 2 h to yield a clear and homogeneous solution. The previously ultrasonically cleaned glass substrates were coated with this solution at 3000 rpm for 30 s and then each layer was heated at 300 °C for 10 min to remove the organic substance. After the ten layers, all the films were annealed at 500 °C for 1 h.

XRD measurements were performed in air with an X-ray powder diffractometer (BRUKER D8 Advance). The diffractometer reflection of all the films was taken at room temperature. The films were mounted on rotating sample holders (15 rpm). A sealed X-ray tube operated at 40 kV and 40 mA with CuKα radiation was used. All measurements were performed in reflection geometry as coupled θ–2θ scans ($30^\circ \leq 2\theta \leq 60^O$) at a divergent slit of 0.5 mm width. Surface morphology was studied using a ZEISS ULTRAPLUS model field emission scanning electron microscopy (FESEM). For the optical transmittance measurements, we used a double beam Shimadzu 2450 UV-spectrophotometer with an integrating sphere in the wavelength range 190–900 nm.

3. Results and discussion

3.1. Structural and morphological properties of the undoped and B doped ZnO films

The XRD patterns of undoped ZnO films for the different pH values are shown in Fig. 1. As shown in this figure, all the films which are polycrystalline with hexagonal wurtzite type structure (Phase zincite, JCPDS card file no: 36-1451) exhibit preferential orientation along the (0 0 2) plane. The ZnO films whose pH value is higher than 5.77 show a high diffraction intensity for the (0 0 2) peak. It is clearly shown that the crystallinity of the films enhances with increasing pH value. This means that the film deposited using the sol of higher pH has more grain growth as compared to the film deposited using the sol of lower pH. Furthermore, the intensity of the (0 0 2) peak increases with increasing pH value. This increase indicates that large amount of volume of crystallites get oriented along (0 0 2) plane.

B doped ZnO films were prepared at pH value of 7.00, because the best film formation was shown at this pH value. So, the effect of doping on the film formation was only studied by keeping constant the pH value. The XRD patterns of undoped and B doped ZnO films at pH = 7.00 are shown in Fig. 2. It is seen that the intensities of (0 0 2) peaks decrease with increasing doping ratio. When differently sized atoms are substituted in the ZnO lattice, some lattice defects and distortion of the crystal lattice may occur [26]. The XRD result suggests that the incorporation of boron atoms leads to a suppression of the crystal growth along the *c*-axis. So, the crystallinity of the films was highly deteriorated with increasing boron content. The intensity of (0 0 2) peak belongs to B doped ZnO films is lower than the undoped. This can be attributed to the formation of stresses by ion size difference between zinc and boron and the segregation of dopants in the grain boundaries.

The variation of Full Width at Half Maximum (FWHM) values with the B content is given in Fig. 3. The FWHM values increase with an increase of B content, which implies the degradation in the crystallinity and the reduction in grain size of the film. The crystallite size (D) of the films was calculated for the (0 0 2) plane to have information about their crystallinity levels. Scherrer's equation [27] was used to calculate the crystallite size of undoped and B doped ZnO films and is given in Fig. 3. The broadened diffraction peaks with increasing B content imply a decrease in crystallite size. In the case of B doping (which is trivalent), the concentration of the zinc interstitials is reduced for charge compensation, resulting in suppressed ZnO grain growth and deteriorated crystallinity [25]. The similar XRD features for B doped ZnO films have been observed by Addonizio and Diletto [17] using low-pressure metalorganic chemical vapor deposition (LP-MOCVD) technique and Kim et al. [26] using liquid source misted chemical vapor deposition (LSMCD) method.

FESEM images for the undoped ZnO films for the different pH values are shown in Fig. 4. All the films show granular structures. It is seen that the grains which belong to the film deposited using the sol with pH value of 7.00 are a bit larger than the others. Fig. 5 shows the effect of B doping on the surface morphologies of the ZnO. It is clearly shown that the surface morphologies of the ZnO were considerably affected by the doping of B. The granular structures are disappearing with doping and the grains are getting smaller with increasing B content. Furthermore, the homogeneities of sur-

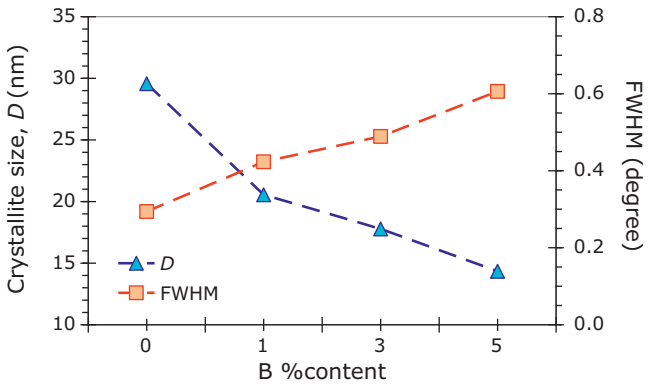

Fig. 3. Variation of crystallite size and FHWM values of the films at pH = 7.00 with the boron content.

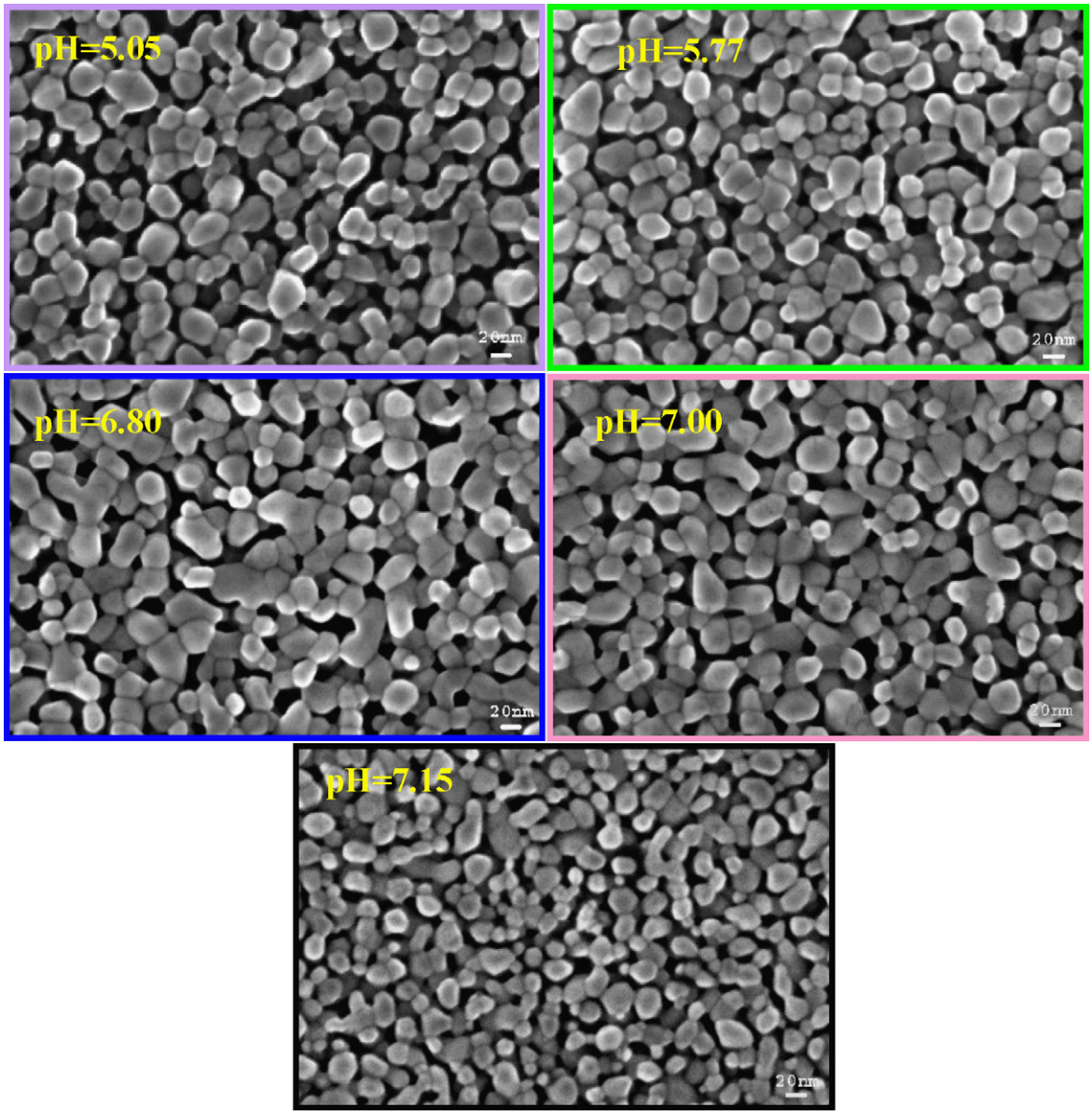

Fig. 4. FESEM micrographs of the undoped ZnO films for the different pH values.

face morphology also disappear. FESEM and XRD analyses contain similar results regarding the effect of doping. Fig. 6 shows cross-sectional view FESEM images of the undoped and B doped ZnO films. These images show that the films are uniform and well adherent to the glass substrates. Film thicknesses measured from the cross sectional FESEM image are found to be within the range of 324–440 nm.

3.2. Optical properties of the undoped and B doped ZnO films

Fig. 7a shows the transmittance spectra of the undoped ZnO films prepared with different pH in the range of 300–800 nm. The average transmittance in the visible region was observed about 85% for the films. Transmittance spectra do not display a fringe pattern in the film obtained at lower than the 6.8 pH value. This means that the film formation is poor in the low pH values. This conclusion supports the XRD results. Fig. 7b shows the transmittance spectra of the undoped ZnO and B doped ZnO films. The average transmittance values decrease with increasing B dopant. The ZnO film shows a higher transmittance than the B doped ZnO films due to a smoother and more uniform surface.

The analysis of the dependence of absorption coefficient on photon energy in the high absorption regions is carried out to obtain the detailed information about the energy band gaps. The optical band gap of the films is determined by the following relation [28]:

$$(\alpha h\nu) = B(h\nu - E_g)^m \quad (1)$$

where B is an energy-independent constant, E_g is the optical band gap and m is an index that characterizes the optical absorption process and it is theoretically equal to 2 and 1/2 for indirect and direct allowed transitions, respectively. $(\alpha h\nu)^2$ vs. photon energy of the undoped and B doped ZnO were plotted and the values of the direct optical band gap E_g values of the films were found. The variation of E_g values depending on the B content is given in Fig. 8. It is seen that E_g values decrease with increasing B content. This decrease in optical band gap (~50 meV) may be possibly due to the existence of B impurities in the ZnO structure, which induce the formation of new recombination centers with lower emission energy. The substitution of B^{3+} with Zn^{2+} increases the carrier concentration. So,

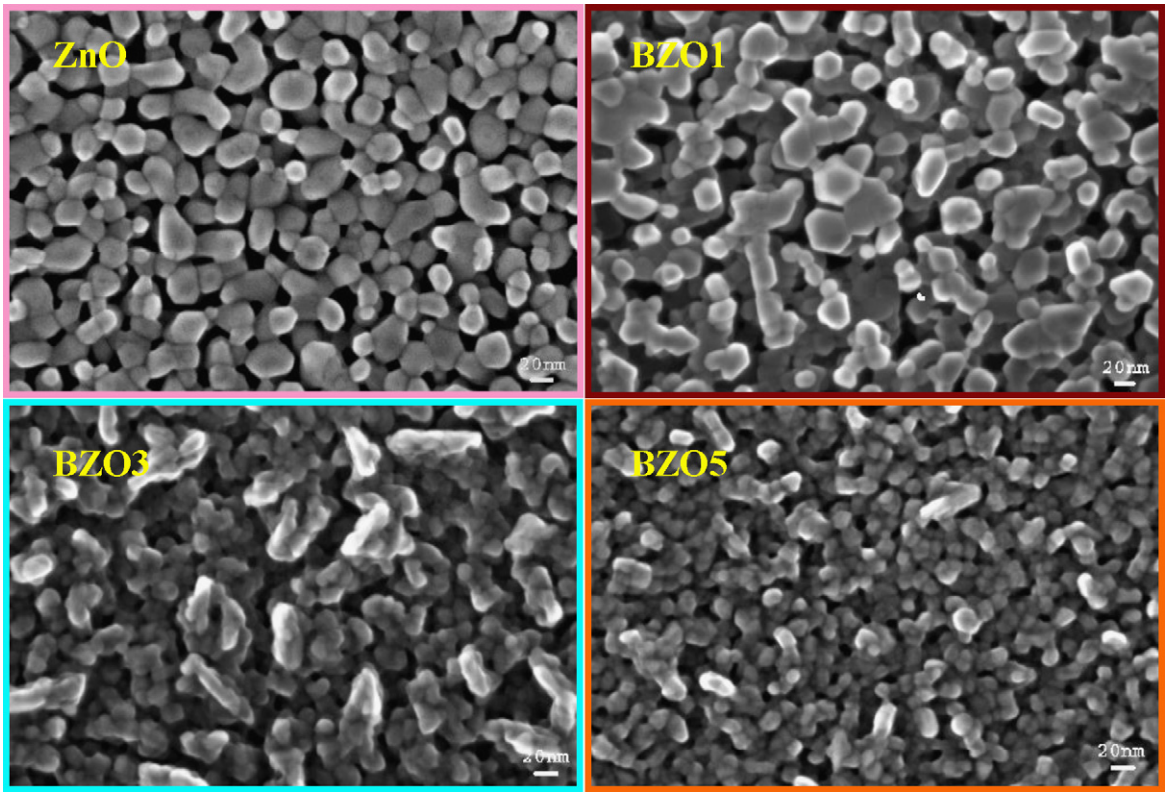

Fig. 5. FESEM micrographs of the undoped and B doped ZnO films at pH = 7.00.

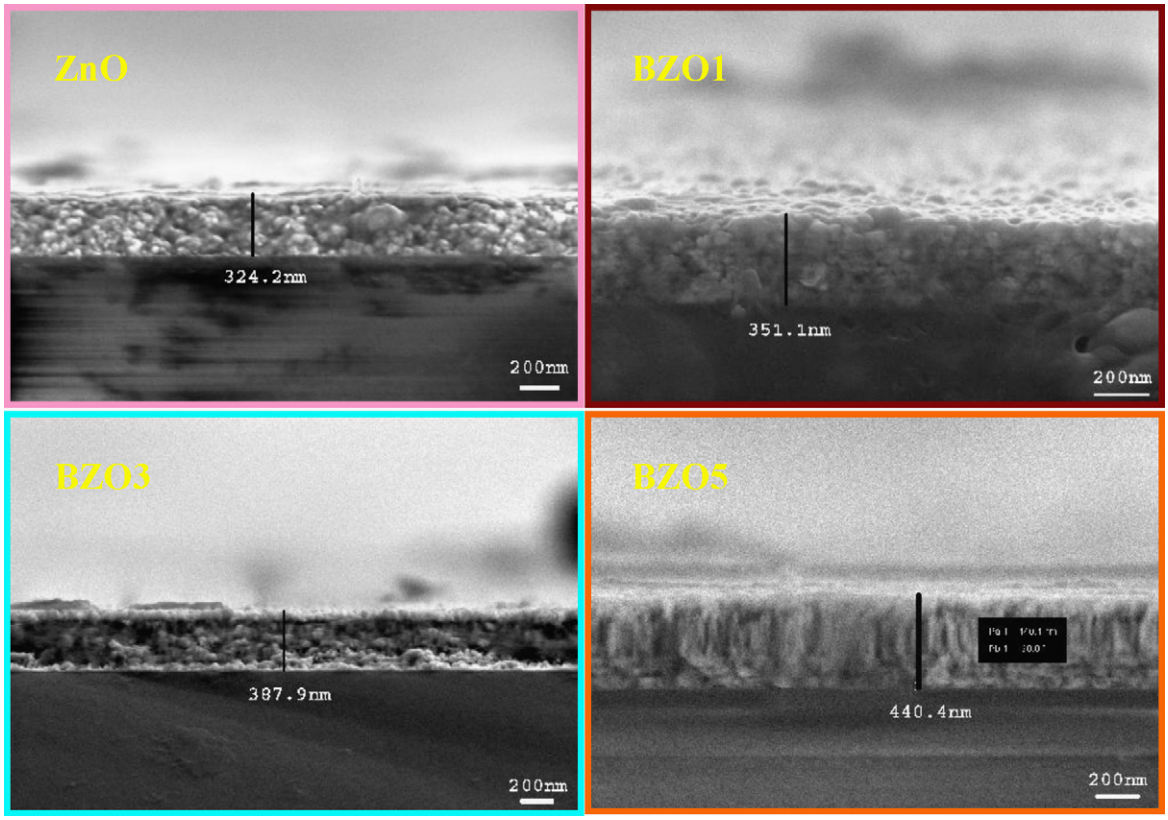

Fig. 6. Cross-sectional FESEM micrographs of the films at pH = 7.00.

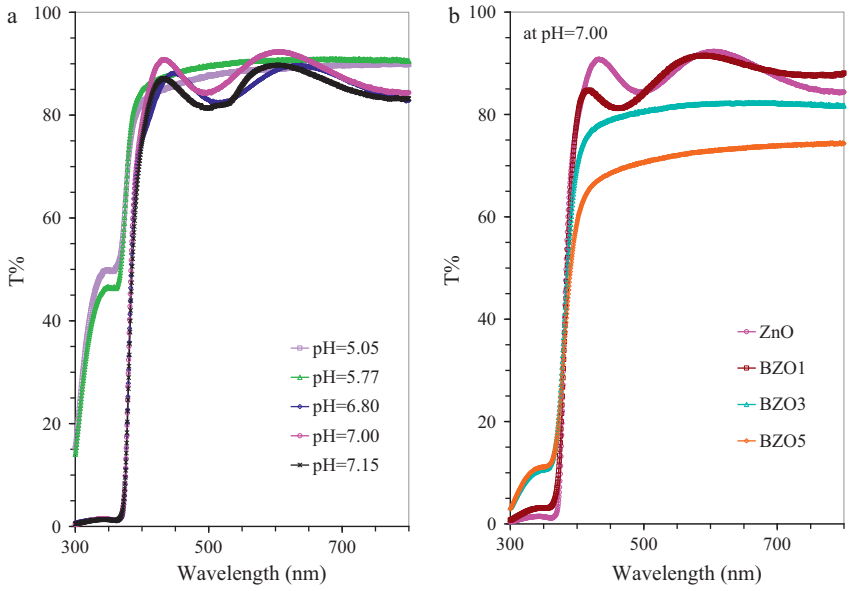

Fig. 7. Transmittance spectra of (a) the undoped ZnO films at different pH values and (b) the undoped and B doped ZnO films at pH = 7.00.

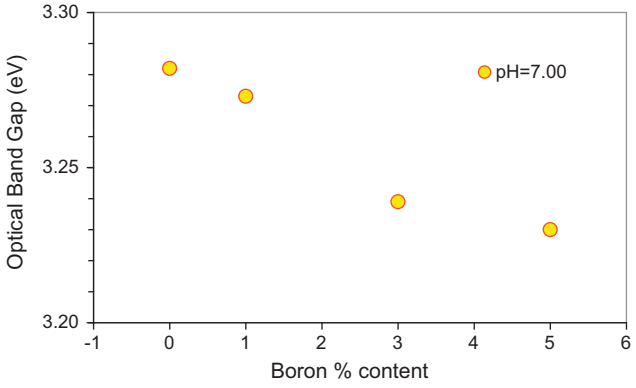

Fig. 8. Variation of the optical band gap values of the films at pH = 7.00 with the boron content.

this increase in the carrier concentration may also cause a decrease in the optical band gap. This may be due to the extension of electronic states of the impurity phase, precipitates and clusters, into the band gap of ZnO.

4. Conclusions

Sol gel method using spin coating technique was used to deposit undoped and B doped ZnO films. The effect of pH on the structural and morphological undoped ZnO films was studied and the optimum pH value was determined for the film formation. So, the effect of doping on the film formation was investigated by keeping constant the pH value. The XRD patterns showed that the crystallinity of the films enhanced with increasing pH value and deteriorated with increasing doping ratio. The FESEM results exhibited that the incorporation of boron affected the surface morphology of the ZnO film. The values of the direct band gap E_g decreased with B content.

Acknowledgements

This work was supported by the National Boron Research Institute (BOREN) (Grant No.: BOREN-2009.Ç0226) and partially supported by Anadolu University Commission of Scientific Research Projects (Grant No.: 081029).

References

[1] C. Yan, L. Nikolova, A. Dadvand, C. Harnagea, A. Sarkissian, D.F. Perepichka, D. Xue, F. Rosei, Adv. Mater. 22 (2010) 1741.
[2] C. Yan, A. Dadvand, F. Rosei, D.F. Perepichka, J. Am. Chem. Soc. 132 (2010) 8868.
[3] C.D. Lokhande, P.M. Gondkar, Rajaram, S. Mane, V.R. Shinde, S.-H. Han, J. Alloys Compd. 475 (2009) 304–311.
[4] C. Leach, N.K. Ali, D. Cupertino, R. Freer, Mater. Sci. Eng. B 170 (2010) 15–21.
[5] D. Calestani, M. Zha, R. Mosca, A. Zappettini, M.C. Carotta, V. Di Natale, L. Zanotti, Sens. Actuators B: Chem. 144 (2010) 472–478.
[6] D. Lee, W.K. Bae, I. Park, D.Y. Yoon, S. Lee, C. Lee, Solar Energy Mater, Solar Cells 95 (2011) 365–368.
[7] G. Xiong, G.A.C. Jones, R. Rungsawang, D. Anderson, Thin Solid Films 518 (2010) 4019–4023.
[8] M. Caglar, S. Ilican, Y. Caglar, Thin Solid Films 517 (2009) 5023–5028.
[9] S. Ilican, Y. Caglar, M. Caglar, B. Demirci, J. Optoelectron. Adv. Mater. 10 (2008) 2592–2598.
[10] M. Caglar, S. Ilican, Y. Caglar, F. Yakuphanoglu, J. Mater. Sci.: Mater. Electron. 19 (2008) 704–708.
[11] H. Zhu, J. Hüpkes, E. Bunte, A. Gerber, S.M. Huang, Thin Solid Films 518 (2010) 4997–5002.
[12] S. Ilican, M. Caglar, Y. Caglar, Appl. Surf. Sci. 256 (2010) 7204–7210.
[13] N. Ye, J. Qi, Z. Qi, X. Zhang, Y. Yang, J. Liu, Y. Zhang, J. Power Sources 195 (2010) 5806–5809.
[14] S. Ilican, Y. Caglar, M. Caglar, F. Yakuphanoglu, Appl. Surf. Sci. 255 (2008) 2353–2359.
[15] Y.-Z. Tsai, N.-F. Wang, C.-L. Tsai, Thin Solid Films 518 (2010) 4955–4959.
[16] X.L. Chen, B.H. Xu, J.M. Xue, Y. Zhao, C.C. Wei, J. Sun, Y. Wang, X.D. Zhang, X.H. Geng, Thin Solid Films 515 (2007) 3753–3759.
[17] M.L. Addonizio, C. Diletto, Solar Energy Mater. Solar Cells 92 (2008) 1488–1494.
[18] C. Avis, S.H. Kim, J.H. Hur, J. Jang, S.J. Hong, J. Korean Phys. Soc. 55 (2009) 255–258.
[19] S. Zhao, Y. Zhou, Y. Liu, K. Zhao, S. Wang, W. Xiang, Z. Liu, P. Han, Z. Zhang, Z. Chen, H. Lu, K. Jin, B. Cheng, G. Yang, Appl. Surf. Sci. 253 (2006) 726–729.
[20] S. Faÿ, J. Steinhauser, N. Oliveira, E. Vallat-Sauvain, C. Ballif, Thin Solid Films 515 (2007) 8558–8561.
[21] B.N. Pawar, S.R. Jadkar, M.G. Takwale, J. Phys. Chem. Solids 66 (2005) 1779–1782.
[22] B.J. Lokhandea, P.S. Patila, M.D. Uplane, Physica B 302–303 (2001) 59–63.
[23] T. Miyata, Y. Honma, T. Minami, J. Vac. Sci. Technol. A 25 (2007) 1193–1197.
[24] B. Houng, C.-L. Huang, S.-Y. Tsai, J. Cryst. Growth 307 (2007) 328–333.
[25] R.B.H. Tahar, N.B.H. Tahar, J. Mater. Sci. 40 (2005) 5285–5289.
[26] G. Kim, J. Bang, Y. Kim, S.K. Rout, S. Ihl Woo, Appl. Phys. A 97 (2009) 821–828.
[27] B.D. Cullity, S.R. Stock, Elements of X-Ray Diffraction, 3rd ed., Prentice Hall, 2001.
[28] J.I. Pankove, Optical Processes in Semiconductors, Prentice-Hall Inc., Englewood Cliffs, NJ, 1971.